Characteristics of DLC films doped with multi-element alloy

Xiuyan Li
Chun-Sheng Chen
Chung-Chen Tsao
Chih-Chung Hu
Cihai Chen
C.Y. Hsu (cyhsu@mail.lhu.edu.tw)
Lunghwa University of Science and Technology, Taoyuan, Taiwan https://orcid.org/0000-0001-7577-018X

Research Article

Keywords: multi-element alloy doped DLC, sputter, TEM, chemical concentration, performance

Posted Date: March 15th, 2022

DOI: https://doi.org/10.21203/rs.3.rs-1425602/v1

Abstract

Multi-element alloy doped diamond-like carbon (DLC) films were coated using sputtering with a (AlCrNbSiTiV) target. TEM and XRD results indicated DLC film had an amorphous compound feature incorporating poly-crystalline phases around the face-center-cubic structure, which were embedded into the amorphous carbon matrix. The Raman spectra and mechanical characteristics of the DLC film sample were associated with concentration changes in the carbon and the multi-element alloy doped in the DLC films, which depended on the DC power. This investigation indicated that improved mechanical properties, including hardness and the elastic recovery rate, can be obtained from the multi-element alloy doped DLC film coated with proper DC sputtering power. These results demonstrated a proper DC power modifies the structure of multi-element alloy doped DLC film and improves its mechanical performance. This study should pave the way for the development of DLC film and elevate its application in various industries.

1. Introduction

Many nanostructured thin films, such as transition metal nitrides (TiAlN, ZrWN, TiN *etc.*) and diamond-like carbon (DLC) films are highly attractive because of their growing application potential and interesting features, including excellent physicochemical characteristics, good biocompatibility and good thermal conductivity [1–3]. DLC films had a mainly amorphous structure, which was composed of sp^3 and sp^2 hybridized C-C and C-H bonded carbon atoms [2, 3]. Controlling the ratio of these components facilitated the optimized properties of films and their wider application [4]. It has been reported that hydrogen-free and hydrogenated DLC nanocomposite films doped with different Al atomic concentrations were fabricated and AlC_x/AlO_x or AlO_x clusters were found in Al-doped DLC films [5]. The Raman spectra for hydrogen-free Al doped DLC composite films showed a typical DLC structure and decreased the sp^3/sp^2 ratio as the Al content increased.

Although improved hardness was obtained, high internal stress resulted in poor adhesion to the substrate, limiting wider applications of DLC films [6]. An alternative strategy was co-doping to reduce residual stress and enhanced the mechanical feature [7]. For example, metallic (W, Nb, V, Mo etc.) and non-metallic (Si, F etc.) elements were co-doped into a carbon bond network of DLC films to increase the surface energy of the film, decrease residual stress and increase adhesive strength [7]. Moreover, doped DLC coatings featured good thermal stability, toughness, and good mechanical and tribological characteristics. Ren et al. [8] reported a boron-doped DLC coating had good fatigue life and tribological properties. A medical apparatus was fabricated using a fluorine-doped DLC film with plasma surface treatment, showing improved biocompatibility [9]. The experimental results showed O-F-DLC film can inhibit the expansion of bacteria. Xu et al. [10] produced Ti-doped DLC films coated with various Ti concentrations using a hybrid ion beam (HIB). Dry tribological tests showed (Ti 4 at.%)-DLC film coating had a very low friction coefficient and a decreased wear rate, due to the formation of transform film and the generation of a carbon graphitized layer in the sliding interface.

DLC films co-doped with multiple elements should have a nanostructure, which is incorporated into the carbon bond films, resulting in improved properties [11, 12]. Ti, Al and V co-doped DLC film decreased the stresses and enhanced the adhesion, which shows well tribological performances [13]. Sun et al. [14] synthesized (Cu, Cr) co-doped DLC films using an HIB system and showed the improved adhesive strength and the elemental content of (Cu, Cr)-DLC films depended on the coating temperature. The exceptional tribological properties of the film were mainly due to the construction of the compact graphitized transfer film.

Moreover, multi-major elements (called high entropy alloys, HEAs) with more than five alloying elements and atomic concentrations from 5 at.% to 35 at.% were also proposed for preparing film coating[15, 16]. Multi-element alloy (AlCrNbSiTiV) have many industrial applications because of a simple solid solution feature and excellent mechanical behavior [17, 18]. Additionally, intermediate metals layer (such as Al, Zr, Ti, Si, Cr) was coated between the film and substrate as an interlayer to decrease residual stress of the film and enhance the adhesion of the DLC films [19].

This work proposes a multi-element co-doped DLC coating, trying to improve the film integrated performance and prolonging the service life of the coated tools with the resulting DLC films. The film was deposited using the reactive direct current (DC) sputtering method with an equiatomic (AlCrNbSiTiV) target. The multi-element alloy layer was used as the interlayer. This study determined the mechanical characteristics, elemental atomic concentration, surface morphology, and structural and adhesive strength of a bilayer multi-element alloy doped DLC sample (with the multi-element alloy film as the interlayer), which was deposited using DC power from 80 to 160 watts. For co-doping DLC films, multiple elements were incorporated into the carbon bond films. A proper DC power should modify the structure of multi-element alloy doped DLC films and improve the mechanical performance.

2. Experimental Procedure

The nearly equiatomic multi-element alloys ($Al_{15.9}Cr_{16.5}Nb_{17.4}Si_{16.1}Ti_{17.1}V_{17.0}$) for this study were fabricated by vacuum arc melting. They were melted at least five times to guarantee chemical element homogeneity. The target was 5 mm thick and 78 mm in diameter with 99.99% purity. Bilayer multi-element alloy doped DLC specimens (with the multi-element alloy film as the buffer layer) were fabricated on silicon wafers (analysis of structure), SUS 304 stainless steel (measurement of adhesion test) and tool inserts (Mitsubishi, TPMN160308-UTi20T, the composition of the tool material, Ti: 8.79 wt.%, Co: 9.34 wt.%, Nb: 6.87 wt.%, W: 75 wt.%) by reactive DC magnetron sputtering using DC power from 80 to 160 watts (step of 20 watts). A mixture of extremely pure 99.99% gases (argon: methane = 80%: 20%) was used for the coating process. The sputtering process used a working pressure of 2.5 Pa, a substrate bias voltage of -30 V, a substrate temperature of 200°C, a target to substrate distance of 75 mm and a coating time of 20 min. The multi-element alloy film interlayer grown with a DC power of 120 watts had a thickness of ~ 163 nm. Prior to coating, the substrate, silicon wafers, SUS 304 stainless steel and tool inserts were cleaned ultrasonically in isopropyl alcohol (IPA) for 15 min, rinsed using DI water, and dried

in nitrogen. Before sputtering, the multi-element alloy target was pre-sputtered for 20 min to eliminate all pollution.

As a precipitation hardening (Al-Zn-Mg-Cu) alloy, 7050 aluminium alloy has been extensively applied in the aerospace industry. Typical material physical features and element components of 7050 aluminium alloy were given in [20]. DLC films co-doped with bilayer multi-element alloy were coated on the cutter inserts for the dry milling operation to determine the wear characteristics. Experiments were performed using a conventional milling machine tool and 7050 aluminium alloy served as the workpiece material (1000 mm in length and 40 mm in width). The milling process used a face milling cutter diameter of 50 mm, spindle speed of 3200 r/min, depth of cut of 3 mm, feed rate of 1800 mm/min and a single tooth cutter inserts without cutting fluid. The surface roughness (Ra) of the machined workpiece (examined by an AFM) and the flank wear for the cutting tool (examined by a SEM) were used to determine wear behavior. All the milling operation were tested three times.

The nano-indentation features of the DLC films sample were performed using a nanoindenter (TriboLab Ubil, Hysirton). The load was increased to a maximum and unloaded to about 80% (holding time of 15 sec) and then unloaded entirely. The indentation depth was about one tenth of the film's thickness. The indentation operation was tested three times. The adhesive characteristics of the DLC film samples were determined using a scratch instrument (J&LTech, JLST022) and a Rockwell indentation test. The surface microstructure, cross-section and multi-element alloy atomic content of the DLC film samples were investigated using a scanning electron microscope (FESEM, 6500 F) instrument with energy dispersive x-ray spectroscopy (EDS). The carbon atomic bonds in the film specimen were analyzed using Raman scattering spectroscopy (Horiba iHR550). Images of the nano-structure of the DLC films sample were obtained using transmission electron microscopy (FEI Tecnai F20, HR-TEM). The properties of the crystal structure of the films were observed using X-ray diffraction (Rigaku-2000). The Cu Kα radiation (λ = 0.1541 nm, 40 kV and 30 mA) had a grazing incidence angle of 1°. The topographical features and surface roughness of the films were determined using an atomic force microscope (PSIA-XE-100, AFM). The frictional features of the DLC films were determined using a pin/ball on disk tribometer (Switzerland, CSM instrument), utilizing a ceramic Al_2O_3 ball (diameter of 6.0 mm) along a circular track of 12 mm diameter, moving at a speed of 18 cm/s, under a load of 5.0 N and with no lubrication. The composition and bond structure of the multi-element alloy doped DLC films were measured using X-ray photoelectron spectroscopy (XPS, VG ESCA Scientific Theta Probe).

3. Results And Discussion

3.1 Surface morphologies and microstructure

Figure 1. shows the cross-sectional SEM morphology of bilayer multi-element alloy (AlCrNbSiTiV) doped DLC samples produced with different DC power settings. The buffer layer (interlayer) is about 163 nm thick. The DLC films grow outwards from the metallic interlayer interface and throughout the layer, which possessed an intense flux, indicating the energy distribution of impinging ions was favorable. The bilayer

film structure is uniform, having a dense morphology without micro-cracks and adhering perfectly. The metallic (AlCrNbSiTiV) interlayer shows a featureless cross-sectional composition structure, increasing the adhesion strength between the film coating and substrate. Moreover, as the DC power increased from 80 to 160 watts, the growth rate of the multi-element alloy doped DLC film increased from 9.40 nm/min (thickness of 188.0 nm) to 25.82 nm/min (thickness of 516.4 nm). Universally, the depositing film should be primarily bombarded by sputtering target atoms, gas ions and plasma gas atoms, and so on, which were closely associated with the sputtering power. The increased energy received from the greater sputtering power should lead to greater particle energy, along with greater bombardment efficiency of the target materials [21]. Therefore, the sputtering energy should significantly affect the deposition rate, along with the increased thickness of the multi-element alloy doped DLC films if the DC power were monotonically increased from 80 to 160 watts.

The effect of the concentrations of C, O and multi-element alloy on the doped DLC sample at various DC power values was examined using EDS. The results are shown in Fig. 2. As the DC power was raised from 80 to 160 watts, the contents of the carbon in the DLC film samples decreased from 57.2 to 43.1 at.%. In contrast, the doping concentrations of the multi-element alloy increased almost linearly. The results indicated the concentrations of carbon and doped multi-element alloy were associated with the doping efficiency due to the varying DC power. A similar trend had been reported that increased sputtering power should decrease the concentration ratio of carbon/metal [22]. A little of oxygen (smaller than 4.2 at.%) was observed for the DLC films, which perhaps were attributed to exposure of the sample in air. Moreover, it should be associated with the residual oxygen in the vacuum chamber because of the relatively high base pressure. The elements Si and Ti were easily bonding due to their low enthalpy to form Si compounds. While the elements Al, Cr, Nb and V are another group to form Al compounds. The deposition rate of Si compoundswas slightly higher than the Al compounds group. So, the metal composition percentage of Ti was slightly higher than the Al. The metal percentages and deposition rate were due to the fact that sputtering power helps to increase the atomic mobility on the growing surface. Different DC power values should result in different degrees of doping with multi-element alloy. However, the relative chemical concentration of the DLC films were similar to that of the multi-element alloy target with an identical DC power due to the similar deposition rate. The concentration of the chemical elements is approximately equiatomic.

The micrographs and phases of the multi-element alloy doped DLC sample were determined using HR-TEM. Figure 3 demonstrates the TEM images of the DLC film corresponding to the selected area electron diffraction (SAED) patterns. It can be observed that a typical nanocomposite structure was formed in the amorphous carbon phases matrix incorporated with metal carbide or metal nanocrystalline. This differs from the DLC coating samples without doping, which showed an amorphous structure without other nano-particulates or crystals [23]. Pauschitz et al. [24] presented the TEM pattern of the composite DLC films, showing a polycrystalline structure. However, as shown in Fig. 3, randomly oriented small grains form multi-element alloy carbide nanocomposites in the amorphous DLC carbon matrix and diffraction rings are also found, which corresponding to the (111), (200), (220) and (311) planes of the face-centered cubic (FCC) structure phase. The results are also verified by XRD measurement below. The metal doped

DLC composite films displayed the FCC crystalline phase, which was in agreement with the results of Li et al. [25]. The crystalline structure and the polycrystalline FCC phase should be associated with the competitive and developmental growth procedure of the multi-element alloy doped DLC coatings. [26]. Figure 4 shows the TEM micrographs and the corresponding mapping of the multi-element alloy doped DLC sample, confirming the doped films have a homogeneous chemical distribution.

Figure 5 shows the AFM and SEM images for the multi-element alloy doped DLC films grown using different DC power values. All DLC films samples showed a relatively smooth nano-particulate structure without delamination, which was homogeneous and had grain-like features on the substrate surface. These results should be relative to the typical carbon-metal structure phase composition clusters in the DLC film [27]. As shown in Fig. 5, DLC films prepared with a low DC power (80 ~ 140 watts) have relatively low surface roughness (Ra = 1.23 ~ 3.02 nm). The surface roughness of film deposited at high DC power (160 watts) has a maximum value of Ra = 4.13 nm. With increased sputtering power, the surface of the films become rougher, which was associated with the agglomeration of nanoparticles due to the increased number of target atoms reaching the substrate within the same time using the greater sputtering power. A similar result was observed in films deposited with sputtering power from 100 to 250 watts [28].

The phase structure of the multi-element alloy doped DLC composite films coated at different DC sputtering power settings was determined by means of X-ray diffraction and shown in Fig. 6. No diffraction peaks relating to the carbon phase are observed, indicating the formation of amorphous carbon matrix in the DLC film. However, the (111), (200), (220) and (311) crystal planes of a nano-grain FCC crystal phase structure can be found in the multi-element alloy doped DLC films sample, which is also confirmed by the TEM topographic images in Fig. 3. Meanwhile, the relative intensity of these diffraction peaks gradually increases with an increase in DC power from 100 to 160 watts. The DLC film samples prepared using a lower DC power exhibited a relatively low XRD pattern and poor crystallinity. It has been reported that a metal-carbon crystalline phase was formed in Ti-doped DLC samples with a high concentration of metal doping, and the fraction of the metal-carbon structure was positively correlated with the content of the metal [29]. Therefore, the low XRD pattern should be attributed to the limited amount of metal atomic of nanoparticles, which would be difficult to uniformly disperse into the amorphous DLC structure due to the lower DC power.

To investigate the chemical composition and bond structure information of the multi-element alloy doped DLC films, analysis of XPS spectra was employed. The high resolution XPS analysis of the Ti 2p, Nb 3d, V 2p, Si 2p, Cr 2p, Al 2p and C 1s regions for the multi-element alloy doped DLC films coated with DC sputtering power of 120 watts, as demonstrated in Fig. 7 (a)–(g). In addition, owing to the signal intensity from the XPS measurement is too low, the hydrogen concentration in the films was neglected, which was also examined by Dai et al. [23]. In Fig. 7(a), the main peak and the others located at ~ 74.8 eV and ~ 75.4 eV corresponding to Al in oxide and Al-O-H bonding situation, respectively, revealed the atom of Al did not bond with C to format carbide. This is also similar to the results of Dai et al. [27]. In Fig. 7(b), binding energy located at ~ 573.8 eV and ~ 575.4 eV were associated with Cr-C/Cr and Cr-O bonding situation,

respectively. Because of the spectra for Cr metallic and Cr in carbide had the same bind energy, resulting in difficult to discern the chemical structures between Cr metallic and Cr carbide [27]. In Fig. 7(c), the different binding energy located at ~ 207.5 eV, ~ 210.3 eV and ~ 208 eV represented Nb-O, Nb-C and NbCO/Nb-O structures bonds, respectively, showed that metallic Nb served as compound of carbide in the DLC samples. As shown in Fig. 7(d), the bonds of Si-C and Si-O showed that the Si elements principally about bonded with C to constitute the Si-C sp^3 structures [23]. Moreover, bonds of Ti-C and Ti-O was located at ~ 459.1 eV and ~ 459.9 eV, respectively, as shown in Fig. 7(e). This result indicated that Ti-doped mainly acted as compound of carbide in the DLC films [30]. As shown in Fig. 7(f), a binding energy at ~ 517.7 eV was related to the oxide structure of V elements. Additionally, from Fig. 7(g), the C1s spectra exhibited C-C/C-H structures and C-O bonds, was located at ~ 284.8 eV and ~ 286.1 eV, respectively.

Raman spectroscopy is used to determine the carbon atomic bonded characteristics of multi-element alloy doped DLC films. The results are shown in Fig. 8. The spectra display an asymmetric dispersion curve with a range of 1000 to 2000 cm^{-1}, which was deconvoluted using Gaussian fitting and had the typical features of a DLC structure [29, 31]. Two resulting deconvoluted sub-peaks were used to express the Raman spectra, implying a remarkable transformation of the carbon bond structure. The D-peak ('disorder') related to the carbon disordered structure (lower wave number at 1335 ~ 1455 cm^{-1}) corresponded to the breathing vibration mode of the sp^2 sites in aromatic rings. The G-peak ('graphite') at a higher wave number (1552 ~ 1580 cm^{-1}) of graphitic carbon was assigned to the bond stretching vibration for all pairs of sp^2 carbon elements in both the aromatic rings and carbon atomic chains [27, 32]. A higher ratio of metallic doping resulted in decreased scattering intensity of the DLC films, which should cause increased sp^2 and less sp^3 content in the metal-doped DLC film [33].

Figure 9 shows the change in the intensity ratio for the D band to G band (I_D/I_G) and the G-peak position of DLC samples with various DC power values. It is seen that the intensity ratio (I_D/I_G) and the G-peak position moderately reduced when the DC power increased from 80 to 120 watts. At a DC power of 120 watts, the minimum values of I_D/I_G and the G-peak position are 0.59 and 1552.2 cm^{-1}, respectively. However, I_D/I_G and the G-peak position value increase as the DC power increases by more than 120 watts. The position of G-peak and the intensity ratios, I_D/I_G, provided qualitative information about the structure of the aromatic rings and carbon chains, which were used to determine the sp^2/sp^3 bonding ratio [34, 35]. The results indicated the increase in DC power from 80 to 120 watts should lead to a decreasing wave numbers shift and decreasing I_D/I_G, which should be associated with the increased sp^3 content along with the reduced (sp^2-C) fraction [36]. At this phase, the consumed sp^2-C in the carbide should be related to the formation of longer metallic-C bonds, leading to increased degree of disorder for the bond arrangement which was linked with higher sp^3 fraction [27]. Inversely, if the DC power was more than 120 watts, the increased I_D/I_G should be attributed to the transform from the sp^3 to sp^2-C fraction. Normally, the increased fraction of distorted bond lengths should result in the increased residual stress. However, the increase of the adatom mobility induced by metal ions bombardment probably relaxed the internal

stress due to the multi-element alloys doping [41]. The results also indicated that the higher DC power would not be conducive to the formation of longer metallic-C bonds.

3.2 Mechanical behavior

Nano indentation was used to determine the surface nano-mechanical behavior of the DLC film samples. The elastic modulus (E, GPa), hardness (H, GPa) and elastic recovery rate (%Re) were determined using a loading and unloading procedure [37]. The Re value represents the capability to resist plastic deformation, which is related to the toughness of the specimen, as defined by Eq. (1):

$$\%\,\mathrm{Re} = \frac{h\max - hr}{h\max} \times 100\% \quad (1)$$

where *h*max is the indentation depth at the peak load and *hr* is the residual depth when the load is removed [37].

Figure 10 shows the load versus displacement curves of nano-indentation tests for bilayer multi-element alloy doped DLC samples grown using different DC power settings. The films show a multiple pop-in event (abrupt displacement burst) due to the interplay between dislocations during the process of elastic-plastic deformation. The pop-ins event was complex and occurred randomly, implying nanoindentation-induced dislocation propagation [38, 39]. In Fig. 10, as the DC power increased, the maximum loading and the Re value increased, reaching a maximum value of 1.60 mN and 62.9%, respectively, at a DC power of 120 watts, and then decreasing as the DC power was increased further. For comparison, the pure DLC and AlCr co-doped DLC sample [27], reported a maximum Re value about 39% and 58%, respectively. The higher Re value should increase the hardness and the adhesion of the films, which was attributed to a change in the crystallite size and relaxation of the elastic strain [40]. Combining with the Raman spectroscopy tests at a DC power of 120 watts, a greater Re value corresponds to a lower I_D/I_G intensity ratio, implying the presence of more sp^3 bonds, which should enhance the hardness property of DLC films.

Qiang et al. [41] presented the stress of the pure DLC thin films was up to about 0.9 GPa. For the low concentration Ti-doped DLC films (Ti concentration was about 0.21 at.%), the stress decreased significantly to 0.3 GPa (almost three times). This significant decrease in internal stress by Ti atom doping should be attributed to the increase of the sp^2-C fraction and distortion of the atomic bond. Compared to the pure DLC, the elastic modulus (E) of the Ti-doped DLC films was decreased from 117 to 97 GPa, and the hardness (H) reduced from 10.5 to 10.3 GPa. Li et al. [42] reported that residual stress, H and E of films were strongly dependent on the concentrations of the co-doped Ti/Al atoms. The doped Ti mainly bonded with carbon and the doped Al existed in oxidation state. As the increase in Ti/Al concentrations, the hard Ti carbide particles were generated following the reduce in sp^2 content, leading to the increase of films hardness, which showed the higher H of 16.4 GPa and E of 178 GPa. Dai et al. [30] proposed the AlTiSi multi-doped DLC films produced with high power impulse magnetron sputtering.

The doped AlTiSi elements concentration was controlled by regulate the Ar fraction in the sputter gas admixture of C_2H_2 and Ar. As a result, the mechanical properties of the coatings enhanced as the Ar fraction increased. It can be seen that the highest E and H value for the AlTiSi co-doped DLC films were 200 GPa and 22 GPa, respectively.

Table 1 summarizes the H, E, I_D/I_G ratio and coefficient of friction (COF) for bilayer multi-element alloy doped DLC samples, which are grown using different DC power settings. Clearly, as the DC power increases from 80 to 120 watts, the H and E values increase to a maximum (H = 17.62 GPa, E = 193.79 GPa) and the I_D/I_G intensity ratio decreases to a minimum, and then decrease (the H and E) and slightly increase (the I_D/I_G ratio), respectively, as the DC power was further increased to 160 watts. Compared with previous reports [41–43], for DLC films sputtered with DC power of 120 watts, a decent mechanical property was obtained using metal doping. The mechanical characteristics of the DLC sample should be associated with the concentration of carbon and doped multi-element alloy, which depended on the DC power. In particular, the mechanical performance of DLC samples was attributed to the sp^3 carbon structure bond inter-link matrix nanocomposite structure. Moreover, a greater sp^3 concentration would lead to higher H and E values [43]. The H^3/E^2 value (resistance to plastic deformation) and the H/E value (resistance against fracture toughness) illustrated the elastic-plastic behavior of hard film [44] and were used to determine the effect of bilayer multi-element alloy doped DLC on the mechanical properties. As shown in Table 1, the H/E ratio is nearly unchanged, but the H^3/E^2 ratio increases from 0.119 to 0.146, if the DC power increased from 80 to 120 watts. However, a different trend was found if the DC power increased further. The results indicated the toughness of the DLC film was enhanced along with reasonable I_D/I_G intensity ratio using a proper DC power. Therefore, a proper DC power enables the coating to better accommodate deformation without cracking. Further, the mechanical characteristics of the DLC film could be optimized by properly adjusting the DC power.

The tribological features of the bilayer multi-element alloy doped DLC films sample were also investigated using a ball-on-disk tribometer. The relation between the slide distance and the COF for DLC samples coated with different DC power settings is shown in Fig. 11. Clearly, the COF changes in the range of 0.38 to 0.61 when applying various DC power values. The DLC specimen coated with a DC power of 120 watts has the lowest COF of approximate 0.38. The results are consistent with the nano-indentation tests, and the small friction coefficient should be associated with greater resistance to plastic deformation due to a proper DC power of 120 watts.

Table 1
Hardness (H), elastic modulus (E), I_D/I_G ratio and coefficient of friction (COF) of bilayer multi-element alloy doped DLC samples coated using different DC power settings.

DC power (watt)	H (GPa)	E (GPa)	H/E	H^3/E^2	COF	I_D/I_G ratio
80	11.57 ± 0.19	114.22 ± 1.84	0.101	0.119	0.61	0.79
100	12.85 ± 0.16	131.56 ± 2.92	0.098	0.123	0.59	0.69
120	17.62 ± 0.13	193.78 ± 3.28	0.091	0.146	0.38	0.59
140	15.82 ± 0.19	177.95 ± 2.49	0.089	0.125	0.49	0.73
160	15.62 ± 0.12	173.41 ± 2.71	0.090	0.127	0.45	0.84

The Rockwell-C adhesion test was adopted to measure the adhesion of the coated films. Jin et al. [45] evaluated six classes (HF1–HF6) of adhesion strength of the coated films. HF1–HF2 and HF3–HF6 denoted sufficient and insufficient adhesion, respectively. In our work, Rockwell C indentation tests were performed using a total load of 1470 N to measure the adhesion of the coated films and the results are shown in Fig. 12 (a). No obvious cracking or peeling around the circumference of the indentation symbol is observed, which is characteristic of the class HF1 adhesive strength of the DLC film grown with a DC power of 120 watts.

Moreover, scratch testing is applied to determine the deformation behavior and adhesion strength of film coatings [46]. The critical scratch load L_{C1}, L_{C2}, and L_{C3} were generally used, which could be identified from the scratch crack patterns [28]. L_{C1} is the critical normal load to characterize the initial crack appearing in the coated specimen. Lc_2 is defined when the film is initial adhesive failure from the substrate surface [47]. Critical load L_{C3} is determined to the loaded at which there is complete delamination of the film. Figure 12 (b) denotes the results of the scratch tracks on the multi-element alloy doped DLC samples. Clearly, cracks were only examined in the scratch track. The L_{C1} load was about 20.1 N and L_{C2} load was about 42.9 N. However, the L_{C3} load was not observed, demonstrating the DLC film had the acceptable adhesion. As reported by Guo et al. [3], the adhesion relation between film layer and substrate, film thickness and coefficient of friction affected the value of critical load. For (Cr, N)-DLC/DLC multilayer films, the respective L_{C1} and L_{C2} were 10.2 N and about 50.0 N, denote that well adhesion strength between coated film and substrates.

Milling operations are used to produce various components. Dry machining did not employ a cutting fluid, thus it has less environment pollution [48]. For coated and uncoated samples, the SEM images of the surface roughness of the machined workpiece and the flank wear of the cutter inserts are illustrated in Fig. 13. Clearly, for cutter inserts with a bilayer DLC coated specimen, the flank wear was significantly reduced from 52.41 ± 1.97 μm to 31.68 ± 2.16 μm (the improvement rate in flank wear is 39.6%) and the surface roughness was reduced from Ra = 3.85 ± 0.29 to Ra = 2.54 ± 0.22 μm (the improvement rate in surface roughness was 34.0%). The decreased flank wear was attributed to the lower surface roughness

and the improved mechanical characteristics because of the helpful multi-element alloy interlayer. The results were consistent with the tribological features and the nano indentation test. This indicates cutting tool inserts coated with multi-element alloy doped DLC film exhibit better machining performance.

4. Conclusions

Bilayer multi-element alloy (AlCrNbSTiV) co-doped DLC film samples with multi-element alloy film as the interlayer were fabricated using reactive DC sputtering with different DC power settings. The DLC films grew outwards from the metallic interlayer interface and throughout the layer, increasing the adhesion strength between the DLC film coating and substrate. Due to the varying DC power, the concentrations of carbon and doped multi-element alloy were associated with the doping efficiency. The metallic (AlCrNbSiTiV) interlayer showed a featureless cross-sectional composition structure, increasing the adhesion strength between the film coating and substrate. The relative chemical concentration of the DLC films was similar to that of the multi-element alloy target elements. With increased DC power, the surface morphology of the films become rougher, which should be related to the agglomeration of nanoparticles. TEM topography of the DLC films showed an amorphous compound along with the formation of metal carbide-nanocrystalline, which had diffraction rings corresponding to the (111), (200), (220) and (311) planes of the FCC structure. This was also verified by the XRD patterns.

As the DC power was raised from 80 to 120 watts, the I_D/I_G intensity ratio and the G-peak position decreased, achieving minimum values and then increasing as the DC power increased further. A lower I_D/I_G intensity ratio resulted in greater H, E and Re values, which should be associated with the sp^3 carbon bond inter-link matrix nanocomposite structure along with better characteristics for the DLC films. XPS analysis indicated that the doped Cr, Nb, Si and Ti elements tended to bond with carbon, while the doped Al and V was related to existed in oxidation state. The Rockwell C indentation and the scratch testing for the DLC film coatings showed good adhesion strength was obtained. After dry milling of an Al alloy 7050 work-piece, the cutting tool inserts coating with a DLC film demonstrate significantly decreased surface roughness and flank wear. These results demonstrated the structure of DLC film should be modified and the mechanical performances of DLC film are improved by using multi-element alloy doping and appropriate DC power.

Declarations

Acknowledgements: The authors gratefully acknowledge the support of the National Natural Science Foundation of China (61975072), Industry-University-Research Collaboration Foundation of the Fujian Province (2020H6017), Natural Science Foundation of Fujian Province in China (2021J011009), Principal Fund of Minnan Normal University (KJ2020029) and the Educational Research Projects for Young and Middle-aged Teachers in Fujian (JT180302, JT180296, JT180303), and Program for Innovative Research Team in Science & Technology in Fujian Province University in China (Optoelectronic Materials and Device Application), and the Ministry of Science and Technology of the Republic of China, through Grant nos. MOST 110-2622-E-262-001, MOST 108-2221-E-262-002-MY2 and MOST 110-2622-E-262-003.

Code availability: Not applicable.

Author contribution: Xiuyan Li conceptualization, **Chun-Sheng Chen** experimentation, **Chung-Chen Tsao** characterization, **Chih-Chung Hu** validation, **Cihai Chen** analysis, **Chun-Yao Hsu** writing - original draft.

Funding: The authors gratefully acknowledge the support of the National Natural Science Foundation of China (61975072), Industry-University-Research Collaboration Foundation of the Fujian Province (2020H6017), Natural Science Foundation of Fujian Province in China (2021J011009), Principal Fund of Minnan Normal University (KJ2020029) and the Educational Research Projects for Young and Middle-aged Teachers in Fujian (JT180302, JT180296, JT180303), and Program for Innovative Research Team in Science & Technology in Fujian Province University in China (Optoelectronic Materials and Device Application), and the Ministry of Science and Technology of the Republic of China, through Grant nos. MOST 110-2622-E-262-001, MOST 108-2221-E-262-002-MY2 and MOST 110-2622-E-262-003.

Data availability: All necessary data is shown in the figures and Tables within the document. The raw data can be made available upon request.

Ethical approval: Not applicable.

Consent to participate: Not applicable.

Consent to publish: Not applicable.

Conflict of interest: The authors declare no competing interests.

References

1. Jing PP, Gong YL, Deng QY, Zhang YZ, Huang N, Leng YX (2020) The formation of the “rod-like wear debris” and tribological properties of Ag-doped diamond-like carbon films fabricated by a high-power pulsed plasma vapor deposition technique. Vacuum 173:109125–109133
2. Melaibari A, AEltaher M (2020) High repetition rate deposition of boron nitride films using femtosecond pulsed laser. Mater Res Express 7:096401–096409
3. Guo CQ, Pei ZL, Fan D, Gong J, Sun C (2015) Microstructure and tribomechanical properties of (Cr, N)-DLC/DLC multilayer films deposited by a combination of filtered and direct cathodic vacuum arcs. Diam Relat Mater 60:66–74
4. Heeg J, Rosenberg M, Schwarz C, Barfels T, Wienecke M (2009) Optimised plasma enhanced chemical vapour deposition (PECVD) process for double layer diamond-like carbon (DLC) deposition on germanium substrates. Vacuum 83:712–714
5. Peckus D, Meskinis S, Vasiliauskas A, Rajackaite E, Andrulevicius M, Kopustinskas V, Tamulevicius S (2020) Structure and optical properties of diamond like carbon films containing aluminium and alumina. Appl Surf Sci 529:147040–147053

6. Imai T, Harigai T, Tanimoto T, Isono R, Iijima Y, Suda Y, Takikawa H, Kamiya M, Taki M, Hasegawa Y, Kaneko S (2019) Shinsuke Kunitsugu, Mikio Ito, Hydrogen-free fluorinated DLC films with high hardness prepared by using T-shape filtered arc deposition system. Vacuum 167:536–541
7. Zhang R, Pu J, Yang Y, Guo L, Wang J (2019) Probing the frictional properties of sulfur-doped diamond-like carbon films under high vacuum by first-principles calculations. Appl Surf Sci 481:1483–1489
8. Ren Z, Chiang R, Qin H, Vasudevan VK, Doll GL, Dong Y, Ye C (2020) Tribological performance of 52,100 steel subjected to boron-doped DLC coating and ultrasonic nanocrystal surface modification,Wear458–459203398–203409
9. Onodera S, Fujii S, Moriguchi H, Tsujioka M, Hirakuri K (2020) Antibacterial property of F doped DLC film with plasma treatment. Diam Relat Mater 107:107835–107842
10. Xu X, Guo P, Li X, Lee KR, Cui P, Wang A (2021) Exploring the tribological behavior of Ti/Al-DLC/PAO/graphene oxide nanocomposite system. Ceram Int 47:11052–11062
11. Ji L, Wu Y, Li H, Song H, Liu X, Ye Y, Chen J, Zhou H, Liu L (2015) The role of trace Ti concentration on the evolution of microstructure and properties of duplex doped Ti (Ag) /DLC films. Vacuum 115:23–30
12. Bouabibsa I, Lamri S, Alhussein A, Minea T, Sanchette F (2018) Plasma investigations and deposition of Me-DLC (Me = Al, Ti or Nb) obtained by a magnetron sputtering-RFPECVD hybrid process. Surf Coat Technol 354:351–359
13. Yetim AF, Kovac H, Kasapoglu AE, Bozkurt YB, Çelik A (2021) Influences of Ti, Al and V metal doping on the structural, mechanical and tribological properties of DLC films. Diam Relat Mater 120:108639–108648
14. Sun L, Guo P, Ke P, Li X, Wang A (2016) Synergistic effect of Cu/Cr co-doping on the wettability and mechanical properties of diamond-like carbon films. Diam Relat Mater 68:1–9
15. Liu YY, Chen Z, Shi JC, Wang ZY, Zhang JY (2019) The effect of Al content on microstructures and comprehensive properties in Al_xCoCrCuFeNi high entropy alloys. Vacuum 151:143–149
16. Biswas K, Yeh JW, Bhattacharjee PP, DeHosson JTM (2020) High entropy alloys: Key issues under passionate debate. Scripta Mater 188:54–58
17. Wan SF, Zuo DL, Hsiao RC, Kao JY, Yu ZH, Hsu CY (2018) Structure and Mechanical Properties of (AlCrNbSiTiV)N Thin Films Deposited Using Reactive Direct Current Magnetron Sputtering. Sci Adv Mater 10:1–6
18. Wu CY, Hsiao RC, Hsu CH, Hsieh TH, Kao JY, Hsu CY (2019) Microstructure and mechanical performance of (AlCrNbSiTiV)N films coated by reactive magnetron sputtering. Bull Mater Sci 42:17–26
19. Shahsavari F, Ehteshamzadeh M, Jamal MRN, Irannejad A (2016) Nanoindentation and nanoscratch behaviors of DLC films growth on different thickness of Cr nanolayers. Diam Relat Mater 70:76–82

20. Sha G, Cerezo A (2004) Early-stage precipitation in Al–Zn–Mg–Cu alloy (7050). Acta Mater 52:4503–4516
21. Dhandapani VS, Kang KM, Seo KJ, Kim CL, Kim DE (2019) Enhancement of tribological properties of DLC by incorporation of amorphous titanium using magnetron sputtering process. Ceram Int 45:11971–11981
22. Bouabibsa I, Lamri S, Sanchette F (2018) Structure, Mechanical and tribological properties of Me-doped diamond-like carbon (DLC) (Me = Al, Ti, or Nb) hydrogenated amorphous carbon coatings. Coatings 8:370–385
23. Dai W, Kwon SH, Wang Q, Liu J (2018) Influence of frequency and C_2H_2 flow on growth properties of diamond-like carbon coatings with AlCrSi co-doping deposited using a reactive high power impulse magnetron sputtering. Thin Solid Films 647:26–32
24. Pauschitz A, Kvasnica S, Jisa R, Bernardi J, Koch T, Roy M (2008) Tribological behaviour of Ti containing nanocomposite DLC films under milli-Newton load range. Diam Relat Mater 17:2010–2018
25. Li H, Hu J, Lin G, Dong C (2010) V and N co-doped diamond-like carbon films deposited by pulsed bias arc ion plating. Int J Refract Metals Hard Mater 28:544–549
26. Tsai DC, Chang ZC, Kuo BH, Lin TN, Shiao MH, Shieu FS (2014) Interfacial reactions and characterization of (TiVCrZrHf)N thin films during thermal treatment. Surf Coat Technol 240:160–166
27. Dai W, Liu J, Geng D, Guo P, Zheng J, Wang Q (2016) Microstructure and property of diamond-like carbon films with Al and Cr co-doping deposited using a hybrid beams system. Appl Surf Sci 388:503–509
28. Jin Y, Wu W, Li L, Chen J, Zhang J, Zuo Y, Fu J (2009) Effect of sputtering power on surface topography of dc magnetron sputtered Ti thin films observed by AFM. Appl Surf Sci 255:4673–4679
29. Zhang M, Xie T, Qian X, Zhu Y, Liu X (2020) Mechanical properties and biocompatibility of Ti-doped diamond like carbon films. ACS Omega 5:22772–22777
30. Dai W, Gao X, Liu J, Kwon SH, Wang Q (2017) Compositionally modulated multilayer diamond-like carbon coatings with AlTiSi multi-doping by reactive high power impulse magnetron sputtering. Appl Surf Sci 425:855–861
31. Pardo A, Aleixandre CG (2011) Metal incorporation strategies in DLC (fullerene-like) thin films grown by ECR-CVD. Vacuum 85:1140–1143
32. Kong W, Yu Z, Hu J (2021) Effect of carburizing treatment on microstructural, mechanical and tribological performances of Cr doped DLC coating deposited on Ti6Al4V alloy. Ceram Int 47:34425–34436
33. Shia X, Guo L, Bai Y, Qiao L (2011) Characterization of coating probe with Ti-DLC for electrical scanning probe Microscope. Appl Surf Sci 257:7238–7244

34. Liu L, Wang T, Huang J, He Z, Yi Y, Du K (2016) Diamond-like carbon thin films with high density and low internal stress deposited by coupling DC/RF magnetron sputtering. Diam Relat Mater 70:151–158
35. Yang W, Guo Y, Xu D, Li J, Wang P, Ke P, Wang A (2015) Microstructure and properties of (Cr:N)-DLC films deposited by a hybrid beam technique. Surf Coat Technol 261:398–403
36. Chen JL, Ji PY, Yang Y, Jin CG, Zhuge LJ, Wu XM (2020) The structure and properties of amorphous diamond-like carbon films deposited by helicon wave plasma chemical vapor deposition. Thin Solid Films 709:138167–138173
37. Wang Q, Zhou F, Zhou Z, Li LKY, Yan J (2017) An investigation on the crack resistance of CrN, CrBN and CrTiBN coatings via nanoindentation. Vacuum 145:186–193
38. Jian SR, Tasi CH, Huang SY, Luo CW (2015) Nanoindentation pop-in effects of Bi_2Te_3 thermoelectric thin films. J Alloys Compd 622:601–605
39. Wang Z, Zhong X, Jiang L, Qi F, Ouyang X, Wang J, Liao B, Luo J (2020) Effect of interfacial delamination on coating crack in thick diamond–like carbon coatings under indentation. Acta Mech Sin 36:524–535
40. Konkhunthot N, Photongkam P, Wongpanya P (2019) Improvement of thermal stability, adhesion strength and corrosion performance of diamond-like carbon films with titanium doping. Appl Surf Sci 469:471–486
41. Qiang L, Zhang B, Zhou Y, Zhang J (2013) Improving the internal stress and wear resistance of DLC film by low content Ti doping. Solid State Sci 20:17–22
42. Li X, Guo P, Sun L, Zuo X, Zhang D, Ke P, Wang A (2017) Ti/Al co-doping induced residual stress reduction and bond structure evolution of amorphous carbon films: An experimental and ab initio study. Carbon 111:467–475
43. He D, He C, Li W, Shang L, Wang L, Zhang G (2020) Tribological behaviors of in-situ textured DLC films under dry and lubricated conditions. Appl Surf Sci 525:146581–146590
44. Santiago JA, Fernandez-Martinez I, Sanchez-Lopez JC, Rojas TC, Wennberg A, Bellido-Gonzalez V, Molina-Aldareguia JM, Monclús MA (2020) Gonzalez-Arrabal, Tribomechanical properties of hard Cr-doped DLC coatings deposited by low-frequency HiPIMS. Surf Coat Technol 382:124899–124909
45. Jin J, Duan H, Li X (2017) The influence of plasma nitriding on microstructure and properties of CrN and CrNiN coatings on Ti6Al4V by magnetron sputtering. Vacuum 136:112–120
46. Cai X, Xu Y, Zhao N, Zhong L, Zhao Z, Wang J (2016) Investigation of the adhesion strength and deformation behaviour of in situ fabricated NbC coatings by scratch testing. Surf Coat Technol 299:135–142
47. Ghabchi A, Sampath S, Holmberg K, Varis T (2014) Damage mechanisms and cracking behavior of thermal sprayed WC–CoCr coating under scratch testing. Wear 313:97–105
48. Liu ZY, Guo YB, Sealy MP, Liu ZQ (2016) Energy consumption and process sustainability of hard milling with tool wear progression. J Mater Process Technol 229:305–312

Figures

Figure 1

SEM cross-sectional morphology for bilayer multi-element alloy doped DLC samples (with the multi-element alloy film as the buffer layer) using different DC power settings: (a) 80, (b) 100, (c) 120, (d) 140 and (e) 160 watts.

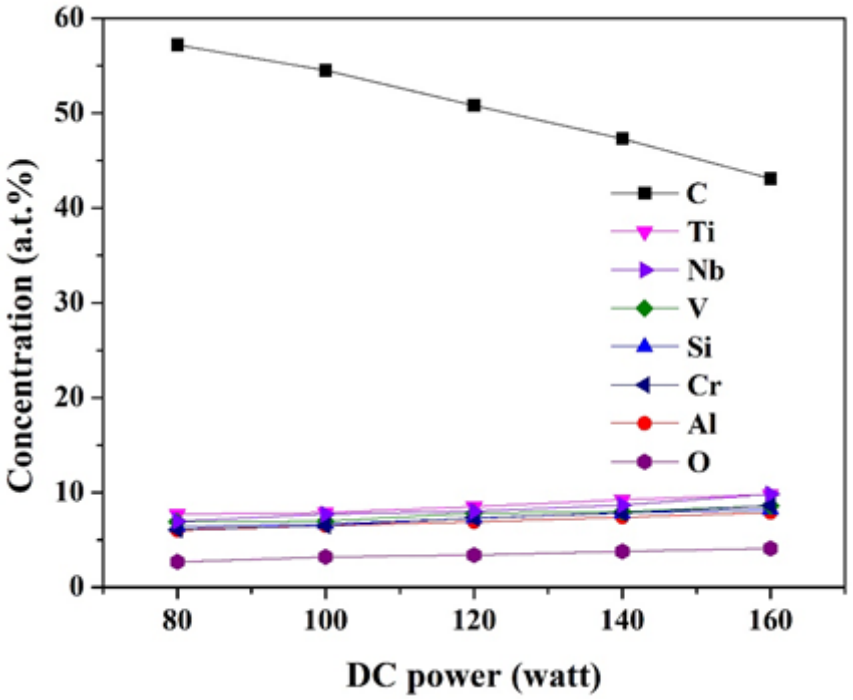

Figure 2

Chemical concentration of the (AlCrNbSiTiV) doped DLC specimen using different DC sputtering power settings.

Figure 3

TEM micrographs of the multi-element alloy doped DLC films coated at a DC sputtering power of 120 watts.

Figure 4

TEM micrographs and EDX for the multi-element alloy doped DLC films coated at a DC sputtering power of 120 watts.

Figure 5

AFM (left) and SEM (right) images for DLC samples (corresponding to Fig. 1) grown using different DC power settings: (a) 80, (b) 100, (c) 120, (d) 140 and (e) 160 watts.

Figure 6

XRD patterns for multi-element alloy doped DLC films coated at different DC sputtering power settings: (a) 80, (b) 100, (c) 120, (d) 140 and (e) 160 watts.

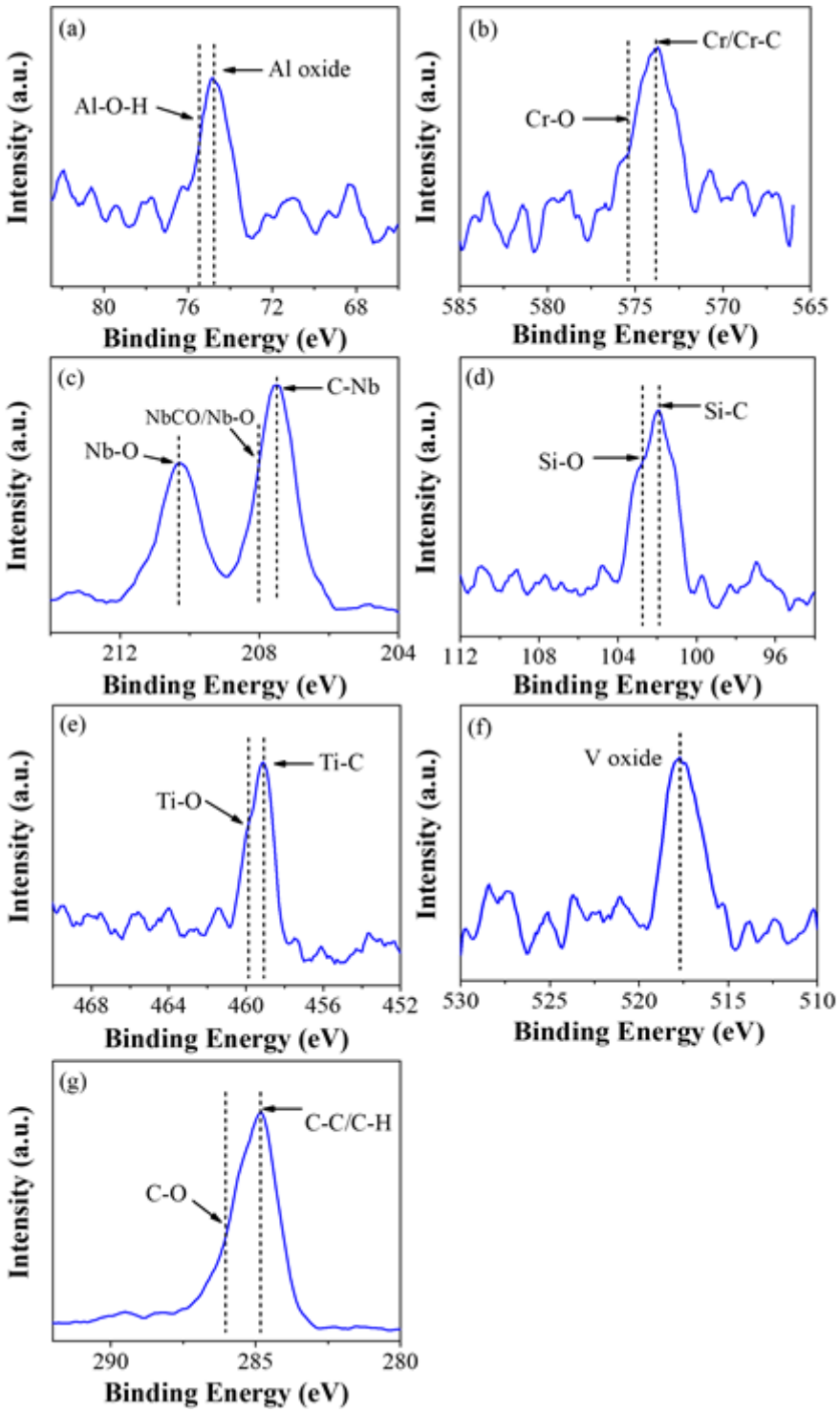

Figure 7

XPS characterization of the multi-element alloy doped DLC films: (a) Al2p, (b) Cr2p, (c) Nb3d, (d) Si2p, (e) Ti2p, (f) V2p and (g) C1s.

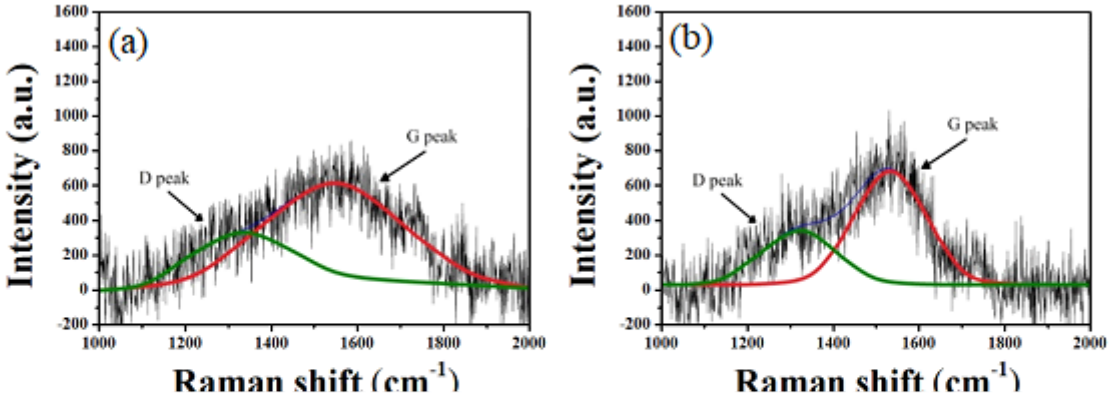

Figure 8

Raman spectra for multi-element alloy doped DLC samples grown using different DC power settings: (a) 80, (b) 100, (c) 120, (d) 140 and (e) 160 watts.

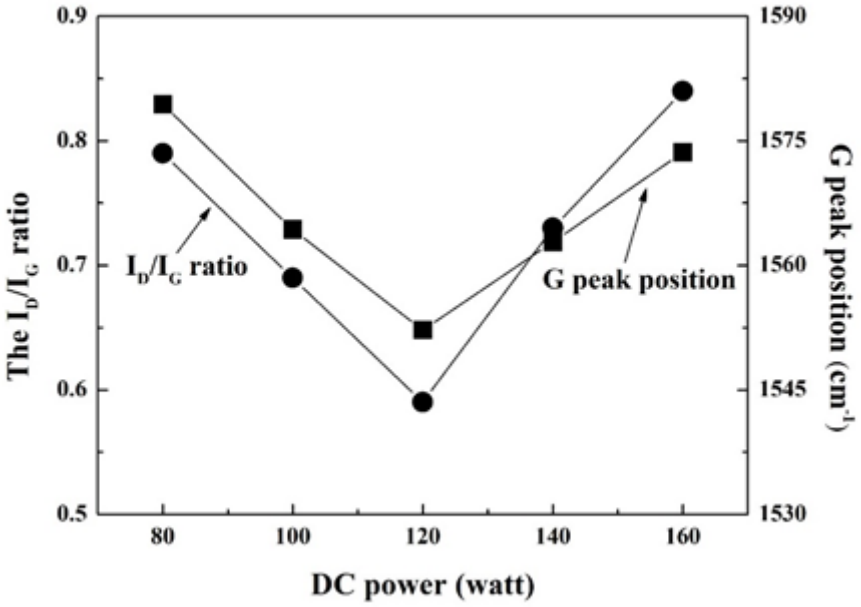

Figure 9

The ratio of I_D/I_G and the position of G-peak for the multi-element alloy doped DLC films grown using different DC power settings.

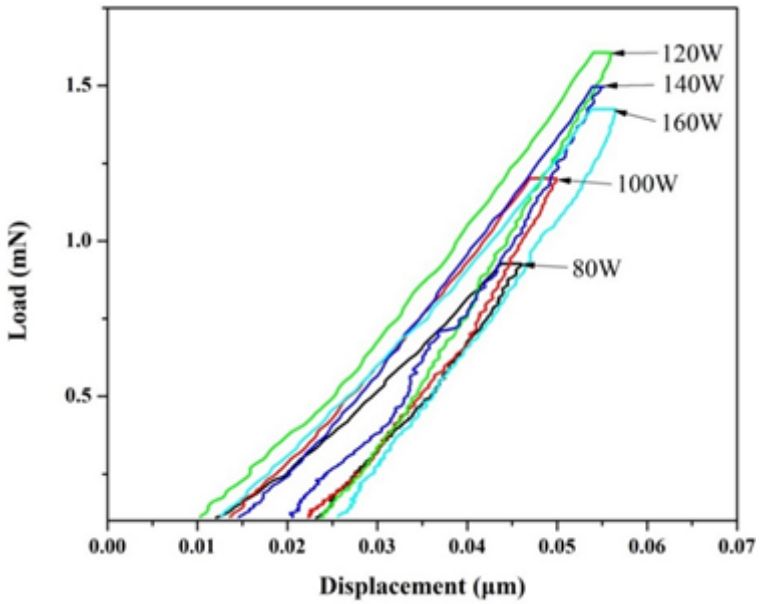

Figure 10

Load versus indenter displacement curves for the nano-indentation tests for multi-element alloy doped DLC samples grown using different DC power settings.

Figure 11

Coefficient of friction of bilayer multi-element alloy doped DLC samples coated using different DC power settings.

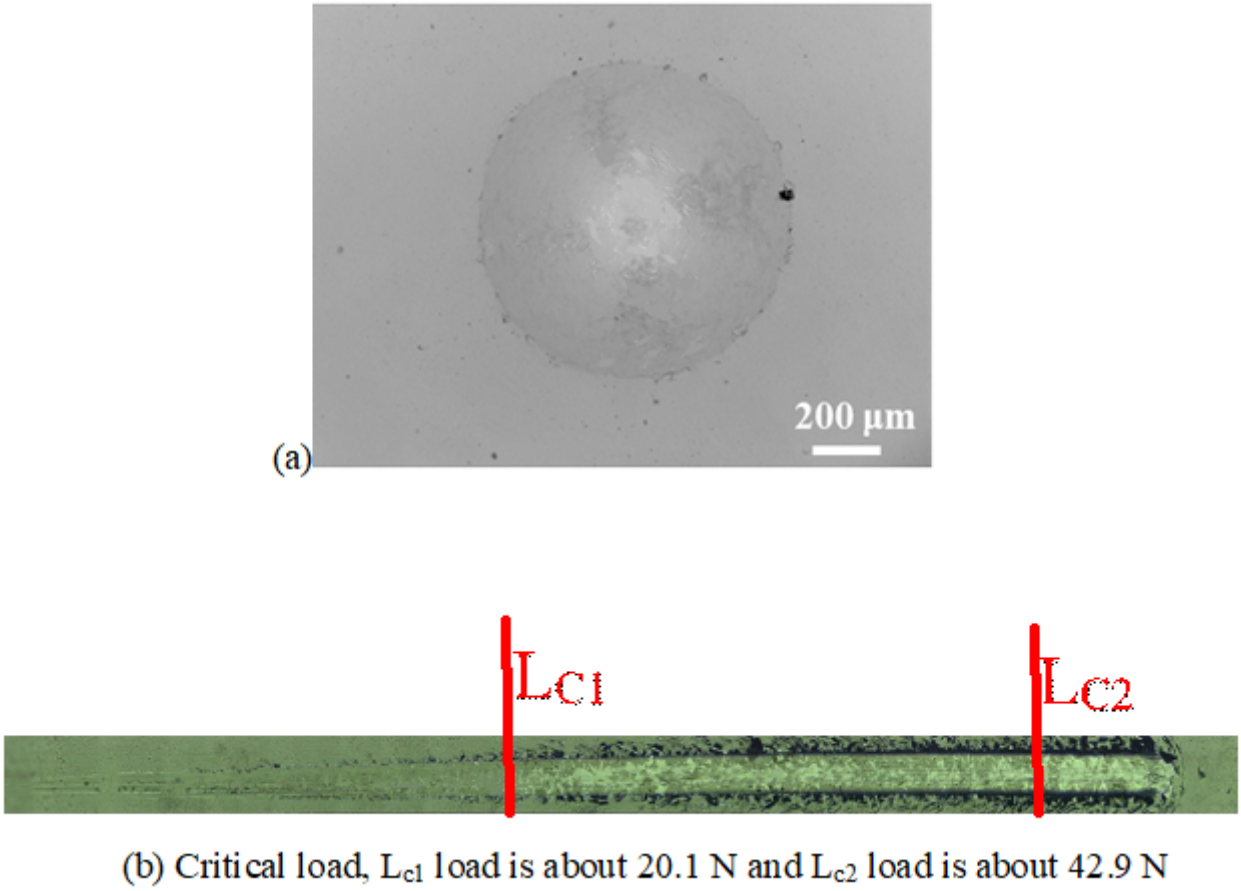

(b) Critical load, L_{c1} load is about 20.1 N and L_{c2} load is about 42.9 N

Figure 12

Fracture morphology for the bilayer multi-element alloy doped DLC films coated with DC sputtering power of 120 watts, measured by (a) Rockwell-C indentation and (b) scratch testing.

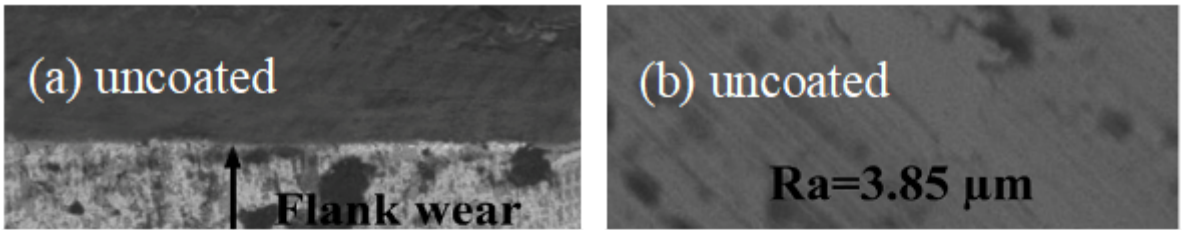

Figure 13

SEM images for the flank wear for cutting tool inserts (left) and the roughness of the machined workpiece (right): (a, b) un-coated cutter and (c, d) cutter inserts coated with a bilayer multi-element alloy doped DLC using a DC sputtering power of 120 watts.